




Article

A Novel Synthesis of a Magnetic Porous Imprinted Polymer by Polyol Method Coupled with Electrochemical Biomimetic Sensor for the Detection of Folate in Food Samples

Sabir Khan ^{1,2} , Ademar Wong ², Michael Rychlik ³  and María del Pilar Taboada Sotomayor ^{2,4,*} 

¹ Department of Natural Sciences, Mathematics, and Statistics, Federal Rural University of the Semi-Arid, Mossoró 59625-900, Brazil

² Institute of Chemistry, São Paulo State University (UNESP), Araraquara 14801-970, Brazil

³ Analytical Food Chemistry, School of Life Sciences, Technical University of Munich, Maximus-von-Imhof-Forum 2, 85354 Freising, Germany

⁴ National Institute of Alternative Technologies for Detection, Toxicological Evaluation and Removal of Micropollutants and Radioactives (INCT-DATREM), Araraquara 14801-970, Brazil

* Correspondence: m.sotomayor@unesp.br

Abstract: The present study reports the development and application of a novel, sensitive, and selective voltammetric sensor for the quantitation of folate or vitamin B₉ in foodstuffs. The sensor was made from magnetic molecularly imprinted polymers (MMIPs), which were synthesized by the core-shell method using magnetite nanoparticles obtained by the polyol method. The MMIP-based sensor was used for the selective and specific detection of folate in different food samples. The MMIP material was constructed using magnetic water-dispersible nanomaterial, which was prepared by immersing iron (III) acetylacetonate in tri-ethylene-glycol (TEG) solvent. The magnetic water-dispersible nanomaterial was then subjected to polymerization using allyl alcohol as a functional monomer, ethylene-glycol-dimethacrylate (EGDMA) as a cross-linking agent, and 2,2-Azobisisobutyronitrile (AIBN) as a radical initiator. The proposed magnetic materials were characterized by Brunauer–Emmett–Teller (BET), field emission gun scanning electron microscopy (FEG-SEM), thermogravimetric analysis (TGA), and vibrating sample magnetometer (VSM) analysis. The quantification of folate was performed by square wave voltammetry under optimized conditions using 15 mg of MMIPs and 85 mg of carbon paste. The modified electrode presented a linear dynamic range (LDR) of 2.0–12 $\mu\text{mol L}^{-1}$ and a limit of detection (LOD) of $1.0 \times 10^{-7} \text{ mol L}^{-1}$ in 0.1 mol L^{-1} acetate buffer solution (pH 4.0). The proposed sensor was successfully applied for folate detection in different food samples, where recovery percentages ranging from 93 to 103% were obtained. Finally, the results obtained from the analysis of selectivity showed that the modified biomimetic sensor is highly efficient for folate determination in real food samples. Adsorption tests were used to evaluate and compare the efficiency of the MMIPs and magnetic non-molecularly imprinted polymer (MNIPs)—used as control material, through the application of HPLC as a standard method.

Keywords: folate; electrochemical sensor; MMIPs; real samples



Citation: Khan, S.; Wong, A.; Rychlik, M.; Sotomayor, M.d.P.T. A Novel Synthesis of a Magnetic Porous Imprinted Polymer by Polyol Method Coupled with Electrochemical Biomimetic Sensor for the Detection of Folate in Food Samples. *Chemosensors* **2022**, *10*, 473. <https://doi.org/10.3390/chemosensors10110473>

Academic Editor: Marco Frascaconi

Received: 26 August 2022

Accepted: 7 November 2022

Published: 11 November 2022

Publisher's Note: MDPI stays neutral with regard to jurisdictional claims in published maps and institutional affiliations.



Copyright: © 2022 by the authors. Licensee MDPI, Basel, Switzerland. This article is an open access article distributed under the terms and conditions of the Creative Commons Attribution (CC BY) license (<https://creativecommons.org/licenses/by/4.0/>).

1. Introduction

Folate or vitamin B₉ refers to a group of water-soluble vitamins and a large number of structurally similar compounds. Folates are essential nutrients that can be synthesized by plant species [1], as well as by some bifidobacterial strains [2] and yeast strains [3–5]. An inadequate folate amount in pregnant and breastfeeding women can lead to birth defects in newborns [6]; the development of cardiovascular diseases [6], cancer, and Alzheimer's disease [7,8]. Folate deficiency has become a prevalent phenomenon in both developed and underdeveloped countries. To effectively tackle this global problem, one needs to have in-depth information on folate content in foods consumed in different regions, as

well as folate bioavailability and folate status worldwide [9,10]. The structure of folates primarily consists of a pterin, para-aminobenzoic acid (pABA), and a wide range of glutamate residues (Figure S1) [1]. The natural forms of folate consist of single carbon derivatives of tetrahydrofolate (H4 folate) and different substituents to N5 or N10. The major sources of folate in food and metabolic reactions are H4 folates, 5-methyltetrahydrofolate (5-CH₃-H4folate), 5-formyltetrahydrofolate (5-CHO-H4folate), 10-formyltetrahydrofolate (10-CHO-H4folate) and oxidized 10-formyl-folic acid (10-CHO-PteGlu), and their inter-conversion products including 5,10-methylenetetrahydrofolate (5,10-CH₂-H4folate) and 5,10-methenyltetrahydrofolate (5,10-CH⁺-H4folate) [10,11]. The multiplicity and complex nature of folate forms and the ability to convert and reconvert them into other forms make the analysis of this group of vitamins extremely challenging. A wide range of methods has been employed for the analysis of folates [12]. Apart from the general extraction procedures, which include extraction in buffer solution, heating, and other clean-up procedures (such as solid-phase extraction), all the methods applied for the analysis of folates require the conversion of polyglutamate folate—the naturally occurring folate in food, into monoglutamate folate through the application of pteroyl polyglutamate hydrolases (PPH) [13,14]. The most commonly applied method for the analysis of folates is the microbiological assay technique. This technique relies on the turbidimetric measurement of bacterial growth for folate determination in which certain bacterial strains require folates for their growth (e.g., *Lactobacillus rhamnosus*) [15]. Chromatographic methods of analysis, such as high-performance liquid chromatography (HPLC) coupled with mass spectrometry (HPLC-MS/MS or LC-MS/MS), have proven to be the most sensitive and accurate techniques for the quantification of folates at trace levels [10–12]. Although they are less commonly employed, biospecific methods are also used for folates determination; these methods of analysis primarily rely on either the use of naturally occurring vitamin-binding proteins and the competitive reaction between folate isomers and folate-binding proteins with limiting numbers of specific binding sites or the specific interaction of an antibody with its antigen (e.g., enzyme-linked immunosorbent assay, ELISA) [15–19]. Even though the microbiological assay facilitates the detection of all folate vitamers, and thus helps to determine the bioactivity of folates, the technique does not allow the differentiation of the vitamers. In contrast, the application of the LC-MS/MS or HPLC-MS/MS methods facilitates accurate differentiation between the vitamers, though the techniques allow one to exclusively quantify the vitamers for which they were calibrated. In addition, as the total folate content is calculated as the sum of all monoglutamates, the application of the LC-MS/MS method allows for the screening of an incomplete deconjugation phenomenon. An incomplete deconjugation phenomenon can lead to an underestimated total folate content when the microbiological assay technique is employed [16]. The analysis of folates remains an extremely demanding task that requires the constant optimization of methods that are specifically tailored for the analysis of folates in different food groups and clinical samples.

In recent years, owing to their outstanding properties, magnetic molecularly imprinted polymers (MMIPs) have been increasingly applied for the analysis of different food and environmental samples. Studies reported in the literature have employed MMIPs for the determination of biotin [20], 4-nitrophenol [21], fluoroquinolones (FQs) [22], sulfonamides [23], glutathione [24], folic acid [25], and tetracycline [26,27].

Taking the above considerations into account, it is clear that the combined application of MMIPs with electrochemical techniques can potentially lead to the development of biomimetic platforms that are highly efficient for the determination of the analyte of interest. Biomimetic sensors are chemical sensors designed to mimic biological systems, as well as their interactions that occur with enzymes and antibodies. In addition to their low cost, Biomimetic sensors can overcome the limitations of enzymes through better analytical performance, either through electron transfer between electrode/biomimetic substrate or through analysis under extreme conditions of pH and temperature. The high stability,

repeatability, selectivity, and sensitivity make these materials highly promising. In this case materials such as MMIPs are ideal for use as biomimetic materials [28].

In the literature, it is possible to find a few works employing electrochemical sensors modified with magnetic MIP. The advantages obtained using these materials are high selectivity and sensitivity and low cost [19,29–31]. Wong et al., developed a screen-printed electrode modified with carbon black (CB) and magnetic Fe₃O₄ nanoparticles coated with a molecularly imprinted polymer (mag@MIP) for the monitoring of a ciprofloxacin antibiotic in the concentration range from 0.5 to 7.0 $\mu\text{mol L}^{-1}$. The proposed method was successful in the determination of ciprofloxacin in river water and synthetic urine samples, with recovery close to 100% [29].

The present work reports the development of magnetic molecularly imprinted polymers (MMIPs) and magnetic non-molecularly imprinted polymers (MNIPs)—used as the control material, and their application for the analytical determination and extraction of folates in food samples. As part of the study of the efficiency of the biomimetic materials proposed here, a selectivity analysis of the sensing technique was also carried out based on the assessment of the peak current intensities of the MMIPs and MNIPs. The function of the magnetic particles is the homogeneous formation of the MMIPs and the formation of a great number of cavities complementary to the analyzed analyte. Thus, allowing for an increase in the performance of electrochemical sensors.

2. Experimental Section

2.1. Materials and Methods

All the chemicals employed in this study were of either analytical or HPLC grade. Some solutions were prepared using deionized water, which was acquired from the Milli-Q Direct-0.3 system (Millipore). Folates, sulphonamides, curcumin, biotin, tetracycline, and folic acid used in the experiments were obtained from Sigma-Aldrich (Brazil). NaOH and HCl, used for pH adjustment, were obtained from Synth-Brazil. Folates Stock/Standard Solution: Stock solution (20 mg L⁻¹) of folates was prepared in 10 mL water. First, the solution was sonicated for 15 min and was then diluted to 100 mL with deionized water. The working solutions were prepared using different concentrations (2, 4, 6, 8, 10, 12, and 14 mg L⁻¹) of the standard stock solution. All other solutions used in the experiments—including sulphonamides, curcumin, biotin, and tetracycline solutions—were prepared in the same way.

Real samples such as beet root, flour, cauliflower, orange, and broccoli were purchased from the local market in Araraquara, which is located in the state of Sao Paulo. For the removal of superficial impurities, the samples were first washed with tap water and sequentially with distilled water and then naturally dried out in the atmosphere of the laboratory. Then, we took 104.11 g \pm 0.1 g of beetroot, 10 g \pm 0.1 g of flour, 70.00 g \pm 0.1 g of broccoli, 58.3 g \pm 0.1 g of cauliflower, 202.41 g \pm 0.1 g of orange and then all were placed separately into a grinder with 100 mL of distilled water then ground it for 10–15 min. Then, 100 mL of water was added and the mixture was homogenized in a blender for 10–15 min. Each sample was heated in the water bath at 50 °C, filtered through qualitative filter paper, and then transferred into a 250 mL volumetric flask, and the level was concluded to the mark through distilled water. A calculated amount of samples was taken and a pH solution of 4.00 maintained for each analysis.

2.2. Theoretical Simulation

Theoretical studies were carried out to select the best functional monomer; to this end, several commonly available monomers were tested due to their affinity toward the analyte. The ORCA (Quantum chemistry Program) software was used for DFT calculations. The hybrid functional B3LYP was used for the DFT calculations and the implicit simulation of the solvent was performed using the COSMO fast and robust approximation salvation model. The calculations were run on the GridUNESP cluster located at the Institute of Theoretical Physics, São Paulo State University (UNESP), in Barra Funda—São Paulo, Brazil.

The DFT calculations were performed using Gaussian 09 program package for different monomers and analytes, as well as for different solvents.

The calculations were performed using M062X hybrid functional—which is superior to other hybrid functionals employed in predicting molecular properties and 6–31++G (d) basis orbitals.

The binding energy (ΔE) was calculated using Equation (1) below. The best energy values obtained for the analyte and monomers are given in Figure 1. As can be observed, allyl alcohol exhibited the maximum interaction energy with the analyte; as a result, it was chosen as the monomer for the preparation of the MMIPs in water (solvent). Some theoretical calculations were also performed for other solvents to select the best solvent.

$$\Delta E = E(\text{folate-monomer}) - E(\text{folate}) - E(\text{monomer}) \quad (1)$$

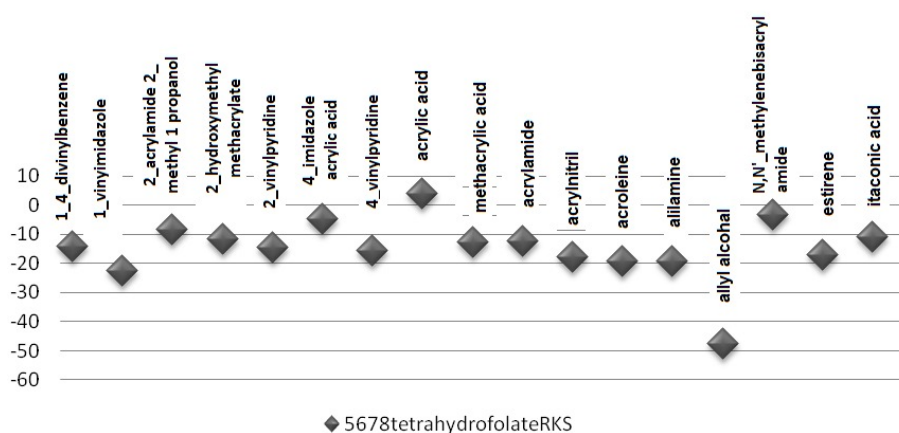


Figure 1. Monomers used for semi-empirical computational simulations.

The best energy values obtained for the analyte and monomers are given in Figure 1. As can be observed, allyl alcohol exhibited the maximum interaction energy with the analyte; as a result, it was chosen as the monomer for the preparation of the MMIPs in water (solvent). Some theoretical calculations were also performed in order to select the best solvent.

2.3. Synthesis of Molecularly Imprinted Polymers

For the conduct of analysis under the polyol method, 4.2 g of iron (III) acetylacetonate, which is commonly referred to as ferric salt, and 80 mL tri-ethylene-glycol (TEG) were mixed; the mixture was then placed in a three-neck round bottom flask equipped with a condenser. The mixture was stirred with nitrogen gas and was heated to 120 °C for 30 min; after that, the temperature was increased to 180 °C and the mixture was heated for 30 min to allow the complete formation of nanoparticles. Finally, the temperature was increased to 280 °C and the mixture was heated again for 60 min. Subsequently, the suspension was left to cool at room temperature, as shown in Figure S2 [32].

Ethyl acetate (60 mL) was mixed with 10 mL of ethanol and the mixture was added to the cooled suspension in order to allow the complete separation of the nanoparticles. In the last step, the mixture was centrifuged and the nano-sized magnetic nanoparticles were separated by an external magnet.

Magnetic molecularly imprinted (MMIPs) polymers were prepared by the polymerization process. The process involved mixing 0.2 mmol of the template (folate), 0.8 mmol of the monomer (allyl alcohol), and 30 mL of ethanol; the mixture was then subjected to continuous agitation using a stirrer for at least 3 h. After that, 200 ± 0.5 mg of the magnetite nanoparticles were added to the mixture, which was further shaken for 3 h at room temperature. The proportion used in the MMIP syntheses presented the best performance in the adsorption tests of the MMIPs concerning the NIP.

Subsequently, 4.0 mmol EDGMA (crosslinking reagent) and 0.05 mmol AIBN (radical initiator) were added to the mixture, which was again subjected to stirring for 12 h at 60 °C (under nitrogen flow) [25,33,34]. Finally, the material was dried under a vacuum to yield a solid product.

After the formation of the polymer, the analyte molecule was removed by Soxhlet extraction using a suitable solvent. The template was removed completely and was tested based on the application of HPLC at 280 nm when no analyte was detected in the eluent. The non-molecularly imprinted magnetic polymers (MNIPs) were also prepared using the same conditions applied for the preparation of the MMIPs but in the absence of the template (folate).

2.4. Electrochemical Measurements

The electrochemical measurements were performed in Autolab[®] potentiostat using Nova[®] v.2 software with a 3-electrode electrochemical cell, which consisted of commercial silver/silver chloride—used as reference electrode (Analion[®]-SP, Brazil), spiral-shaped platinum wire used as auxiliary electrode, and the modified carbon paste electrode used as a working electrode. All the experiments were carried out at room temperature (25 ± 1.0 °C).

2.5. Preparation of the CPE Modified with MMIP

The carbon paste electrode (CPE) was modified using an amount of modified paste (obtained from the mixture of 15 mg of Fe₃O₄@MMIP, 85 mg graphite, and 80 mg mineral oil). The dimension of the cavity of the carbon paste electrode used was 1.5 mm in diameter and 1 mm deep. The electrode surface was polished with a clean paper sheet before taking the electrochemical measurements and the same procedure was used for the renovation of the surface. The proportion of the mass of graphite powder and MMIP tested was 10:90, 15/85, and 20/80 (m/m) being the mixture made using a mortar and pestle for a time of 15 min.

2.6. HPLC-UV Analysis

High-performance liquid chromatography (HPLC) was performed using Shimadzu HPLC 20A, equipped with an automatic injector (model SIL-20A), quaternary pump, degasser system (model DGU-20A5), and UV detector (model SPD-20A). Chromatographic separation was carried out using a reversed-phase C18 column (4.6 × 250 mm, 5 μm) Shim-pack CLC, Shimadzu. The diode array detector (DAD) employed was based on the absorption of ultraviolet light or visible light by the sample components when subjected to electromagnetic radiation.

The mobile phase was composed of a mixture of methanol and phosphoric acid in the volumetric ratio of 60:40 *v/v*, respectively. The flow rate was adjusted to 1.0 mL min⁻¹ and the detector was operated at the wavelength of 280 nm.

3. Results

3.1. Textural Properties of Polymers

Nitrogen adsorption–desorption analysis was used to evaluate the porosity based on N₂-sorption isotherms at 77 K using Micro metrics GEMINI VII 2390 t instrument for MMIPs and MNIPs, and the results obtained are shown in Table 1 and the graphs for nitrogen adsorption in Figure S3. As can be observed, the surface area of the MMIPs was found to be larger than that of the MNIPs (165.76 m²/g and 34.82 m²/g, respectively); this is attributed to the cavities that were formed in the imprinted polymer after the removal of the analyte [35]. In addition, the MMIPs exhibited relatively larger pore volume and pore size compared to the MNIPs; this explains why the MMIPs recorded higher adsorption capacity for folates compared to the MNIPs.

Table 1. Fe_3O_4 @MMIPs and Fe_3O_4 @MNIPs surface area and porosity based on the application of the BET method.

Polymer	BET Surface Area (m^2/g)	Pore Volume (cm^3/g)	Maximum Adsorption (cm^3/g)
MMIPs	165.76	0.37	57.25
MNIPs	34.82	0.12	11.84

3.2. Morphological Characterization

The surface structure and homogeneity of the iron and iron core–shell materials were analyzed using scanning electron microscopy (SEM) analysis.

Figure 2A–C shows the surface morphology of the modified materials—including the magnetite nanoparticles—as well as the MMIPs and MNIPs. The SEM images show homogeneous particles with well-defined shapes as well as rounded surfaces which are attributed to the application of the polyol method rather than the traditional co-precipitation method for the synthesis of the materials.

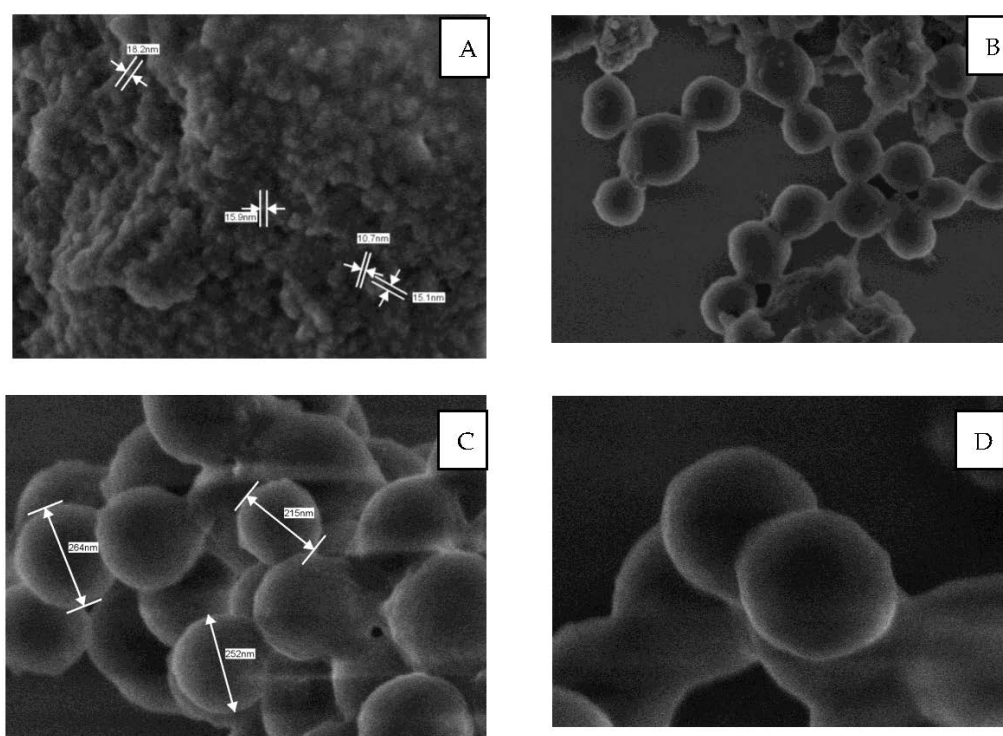


Figure 2. SEM images of (A) magnetite nanoparticles (Fe_3O_4), (B) magnetite nanoparticles modified with silica Fe_3O_4 @ SiO_2 , (C) MMIPs, and (D) MNIPs prepared using the polyol method.

Figure 2A shows nanosized magnetite nanoparticles (Fe_3O_4) with clear, homogeneous surface textures. The images obtained for the magnetite Fe_3O_4 nanoparticles show a crystal size of 8–15 nm with mostly uniform structures and monodisperse distribution. The average size of the images of Fe_3O_4 @ SiO_2 was increased when compared with the calculated size of Fe_3O_4 nanoparticles, which were $115.00 \text{ nm} \pm 11.00 \text{ nm}$ using image-J software. The images of the MMIPs and MNIPs have an almost similar size of $250 \text{ nm} \pm 15.00$ and show more rounded, spherical nanoparticles with an identical size; these nanoparticles act as a unique substrate for the nanostructured, imprinted materials. The uniform surface of the MMIPs exhibits well-defined cavities with several suitable sites for the adsorption of folate. The MMIPs were found to be considerably more porous and granular compared to the MNIPs (used as control polymer); this has already been confirmed by the differences in the size of the surface area of the two polymeric materials.

3.3. Transmission Electron Microscopy (TEM) Analysis

Figure 3 shows the TEM images of the polymer layers around the iron nanoparticles. These core-shell-like iron nanoparticles exhibit equally dispersed size distributions. The morphological analysis of the MMIP and MNIP samples showed that the polymers exhibited a rounded/spherical shape with minimal aggregation of nanoparticles and lesser irregularity in shape. An increase in the average particle size of the materials was observed after polymerization. The presence of a higher amount of the metal precursor, regardless of its nature, was also found to cause an increase in the size of the particles; this observation was previously reported in studies involving the synthesis of magnetite nanoparticles using the thermal decomposition method [36,37].

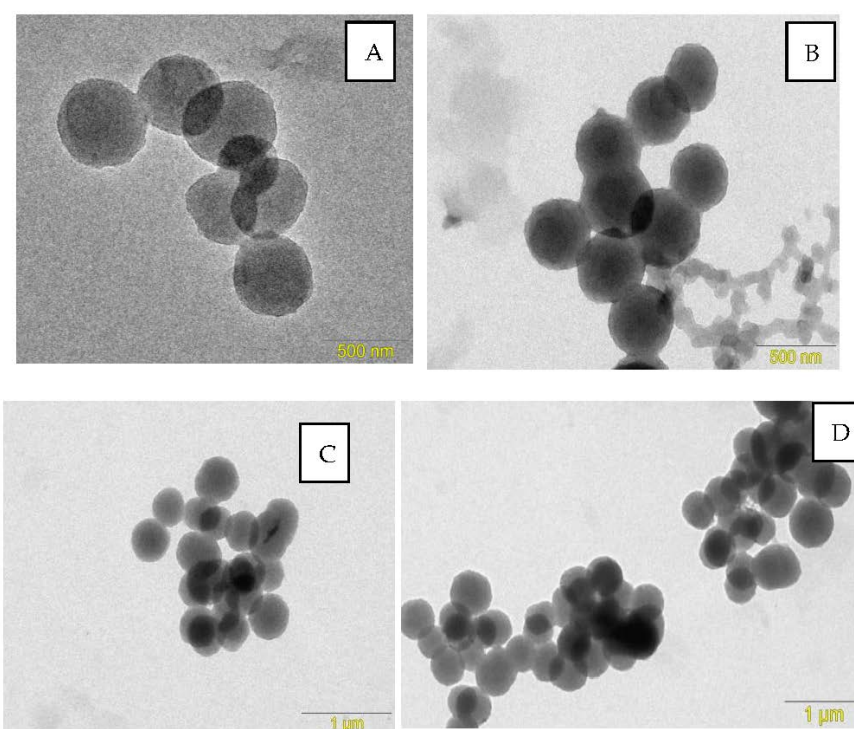


Figure 3. TEM micrograph of the modified magnetite nanoparticles, (A,C) MMIPs, and (B,D) MNIPs.

3.4. Thermogravimetry (TGA) Analysis

The analysis of thermogravimetry provides us with a clear understanding of the changes in the mass of the materials caused by changes in temperature or time. This analysis also helps specifically evaluate the occurrence of material decomposition, as well as the oxidation reactions and physical changes that occur in the materials during processes such as sublimation, vaporization, and desorption.

Thermogravimetry analysis is also exceptionally useful for the study of smart, polymeric materials, including thermoplastics, thermosets, elastomers, composites, films, fibers, coatings, and paints [38]. Thermal steadiness/stability is an outstanding property of polymers which makes them suitable for application in various fields. Thermogravimetric curves help elucidate the decomposition mechanism of the polymers. This decomposition profile defines the characteristics of the polymer and aids in its identification. Figure 4 shows the results obtained from the application of the TGA; as can be observed, both the MNIPs and MMIPs exhibited almost similar thermal behavior. Both polymeric materials exhibited water loss up to 100 °C. The decomposition of the MNIPs and MMIPs occurred at 328 °C and 364 °C, respectively, and the exothermic heat flow for the MNIPs and MMIPs was observed at 445 °C and 459 °C, respectively. The MMIPs needed higher temperatures to operate; this was probably because there were still some folate molecules in the polymeric

structure, which led to an increase in the decomposition temperature. Overall, the results show that the MMIPs and MNIPs are stable at high temperatures [39].

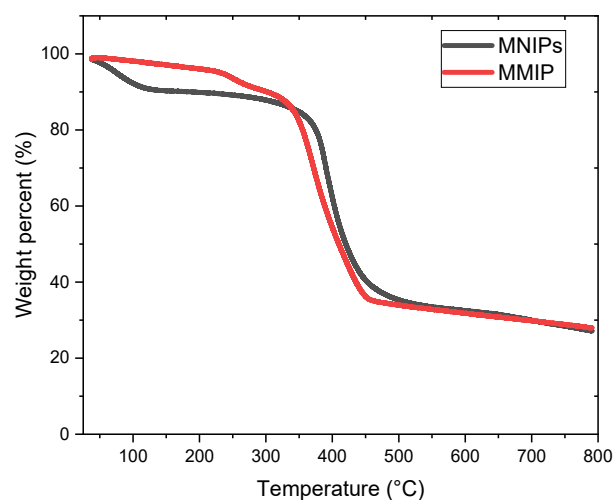


Figure 4. Thermogravimetric analysis plots of the MMIPs (black) and MNIPs (red) were obtained under a nitrogen atmosphere.

3.5. Vibrating Sample Magnetometry (VSM)

The magnetic properties of the biomimetic materials were investigated using magnetization curves (Figure 5). The results obtained showed that all the magnetic materials exhibited magnetic behavior at 300 K. Vibrating sample magnetometry (VSM) was used to study the magnetic properties of the synthesized magnetic materials, as illustrated in Figure 5. It is noticeably evident that there is no hysteresis and both the remanence and coercivity of the materials are zero; this implies that the magnetic samples investigated are superparamagnetic [31,32,40]. The decrease in magnetic behavior may be attributed to the introduction of a small particle surface effect with an inactive magnetic layer, which has a spin that shows no co-linearity with the magnetic [41–43]. The magnetic value of the MMIPs was found to be almost similar to that of the MNIPs though it was much smaller than that of the magnetite nanoparticles—this proved to be effective in magnetic separation.

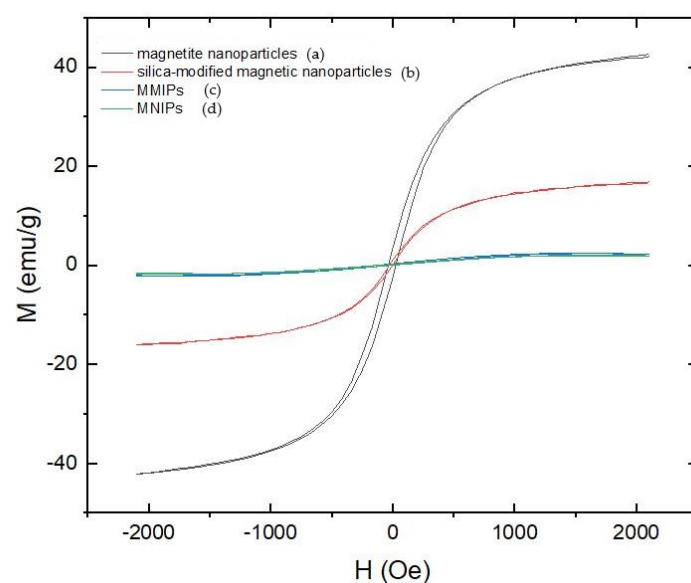


Figure 5. Hysteresis loop of the (a) synthesized magnetite nanoparticles (magnetite), (b) silica-modified magnetic nanoparticles, (c) MMIPs, and (d) MNIPs.

3.6. Construction of Analytical Curve for HPLC

The calibration curve was constructed using HPLC-UV (Figure S4) with different folate concentrations; this was carried out for comparison purposes. The HPLC curve showed that an increase in the signal area was proportional to an increase in the analyte concentration, with a linear range from 2.0 to 12.0 ppm. Figure S4 shows the standard chromatogram illustrating the chromatographic conditions with a retention time of 2.57 min. The analysis of the calibration curves pointed to a good linearity range and satisfactory correlation coefficients (r); this shows that the linear regression perfectly fits the experimental data (a linear response was obtained over the concentration range tested).

Figure 6 shows a comparable chromatogram obtained from the application of the standard solution at 10 ppm for the MMIPs and MNIPs under the same experimental conditions. Figure 6(a) shows the standard solution, Figure 6(b) shows the MNIPs, and Figure 6(c) shows the MMIPs after adsorption. The results obtained showed that the MNIPs adsorbed only 9% of the analyte, while the MMIPs adsorbed 98% of the analyte (based on the application of standard solution at 10 ppm). Thus, compared to the MNIPs (control polymer), the MMIPs exhibited significantly greater analyte adsorption; this is attributed to the selective cavities present in the molecularly imprinted material, which are inexistent in the control polymer.

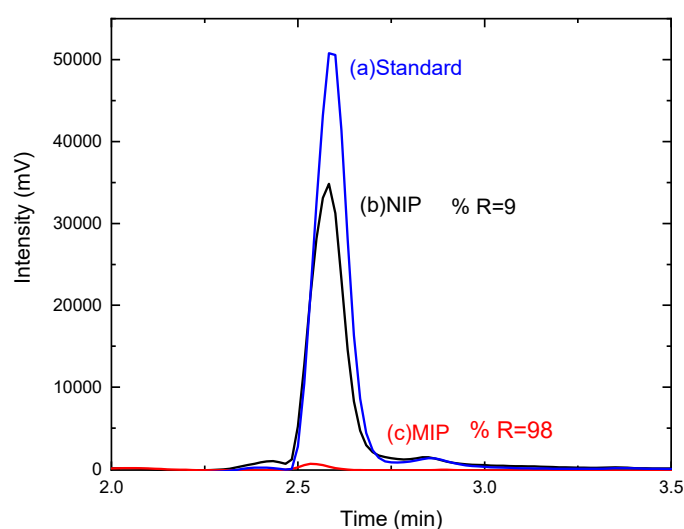


Figure 6. HPLC spectra obtained for the standard material (a), MMIPs after adsorption (b), and MNIPs (c). Conditions applied: methanol: phosphoric acid in the ratio of 60:40; wavelength: 280 nm.

3.7. Using Square Wave Voltammetry (SWV) for the Analysis of the Electrochemical Profile of the Electrodes

A thorough analysis of the electrochemical performance of the electrodes was conducted by cyclic voltammetry (CV) using a carbon paste electrode (CPE), MNIPs/CPE, and MMIPs/CPE in the presence of $1.1 \times 10^{-5} \text{ mol L}^{-1}$ of folate solution. Figure S5 shows the results obtained from this analysis. As can be observed (Figure 7), the MMIPs/CPE sensor exhibited the best electrochemical response, with an electrochemical signal 4.0-times greater than that of the MNIPs/CPE sensor and much higher than that of the CPE. The significant increase in the signal of the MMIPs/CPE is attributed to the excellent interaction between the specific cavities (with a high surface area) present in the polymeric material and the analyte in the solution. The outstanding performance of the MMIPs/CPE can thus be linked to its highly selective adsorption of the analyte; the CPE exhibited no such behavior, while the MNIPs/CPE exhibited low adsorption.

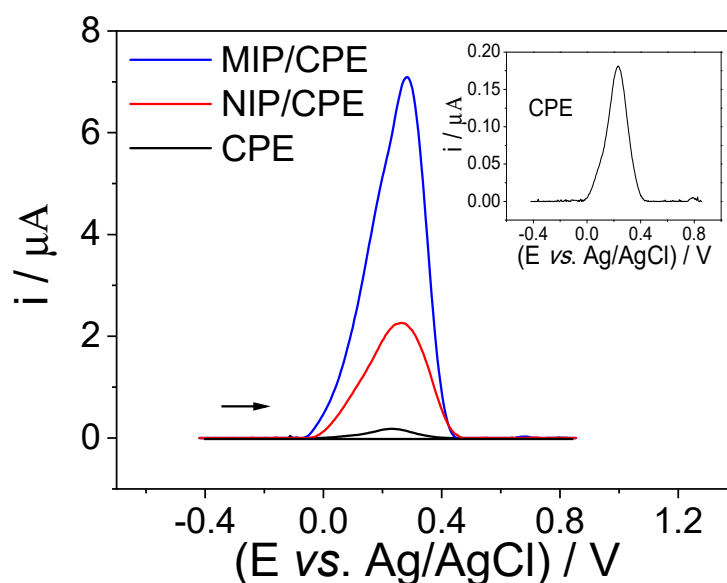


Figure 7. Square-wave voltammograms obtained for the modified electrodes. Analysis conditions: 0.1 mol L^{-1} acetate buffer solution (pH 4.0). SWV conditions: $f = 15 \text{ Hz}$, $a = 75 \text{ mV}$, $\Delta E_s = 5 \text{ mV}$ and $[\text{folate}] = 2.2 \times 10^{-5} \text{ mol L}^{-1}$.

The electrochemical profile of the electrodes was also evaluated using the square wave voltammetry (SWV) technique. The results obtained were very similar to those obtained under the application of cyclic voltammetry. The MMIPs/CPE, MNIPs/CPE, and CPE exhibited the following current signal values: $7.1 \mu\text{A}$, $2.2 \mu\text{A}$, and $0.17 \mu\text{A}$, respectively. Thus, the results obtained from the application of both cyclic voltammetry and square wave voltammetry pointed to similar electrochemical behavior of the modified electrode. The outstanding advantages of the proposed electrochemical technique include the following: (i) the direct detection of an analyte in solution; (ii) a high degree of constancy and reproducibility; (iii) low cost; and (iv) the ability to conduct consecutive analyses with the electrode by simply polishing the electrode surface [25,34].

Figure 8 shows the results obtained from the application of square wave voltammetry (SWV) for the electrochemical determination of folate. The quantification of folate is carried out through successive addition in the presence of 0.1 mol L^{-1} acetate buffer at pH 4. In preliminary tests, Britton–Robinson buffer was tested at different pHs (2–10) and it was found that pH 4 showed a better analytical signal. When compared with acetate buffer at the same concentration, acetate buffer showed a better response and was therefore used as the buffer in the following studies. It is worth mentioning that the pre-concentration did not present significant results in the electrochemical analyzes in the presence of folate.

Under the best analysis conditions, we obtained a concentration linear range of 4.4 to $26.4 \mu\text{mol L}^{-1}$ and a limit of detection of $1.0 \times 10^{-7} \text{ mol L}^{-1}$ —this was obtained from the application of $3\sigma/\text{slope}$ ratio. The results obtained with this method showed an analytical performance superior to those obtained with the chromatographic methods.

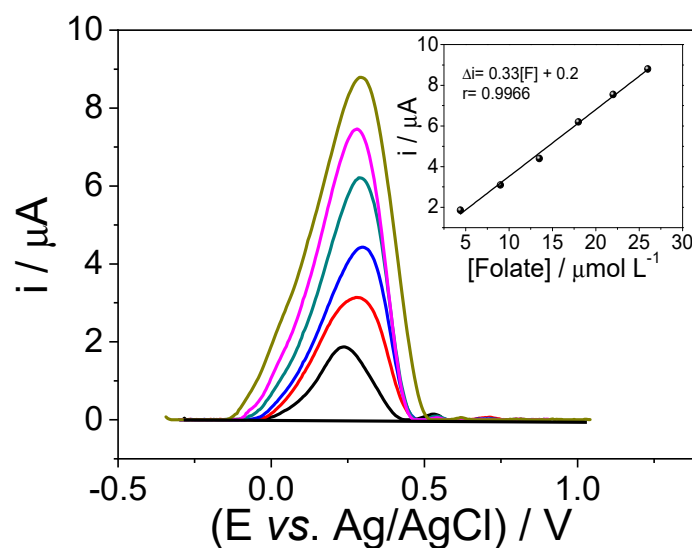


Figure 8. Electrochemical determination of folate by SWV using the mag-MIP/CPE sensor. Analysis conditions: 0.1 mol L^{-1} acetate buffer solution (pH 4.0). SWV conditions: $f = 15 \text{ Hz}$, $a = 75 \text{ mV}$, $\Delta E_s = 0.005 \text{ mV}$.

3.8. Repeatability of MMIPs/CPE

The repeatability analysis of the MMIPs/CPE sensor was performed using $0.7 \mu\text{mol L}^{-1}$ concentration of folate in 0.1 mol L^{-1} acetate buffer (at pH 7.0) with the same electrode, consecutively (Figure S7). The relative standard deviation (RSD) obtained in the five electrochemical measurements was 0.9%. The electrode stability was also performed for 21 electrochemical measurements on CV and SWV in the absence and presence of folate. The stability of the electrochemical signal can be shown in Figure 9, with a standard deviation of less than 4%.

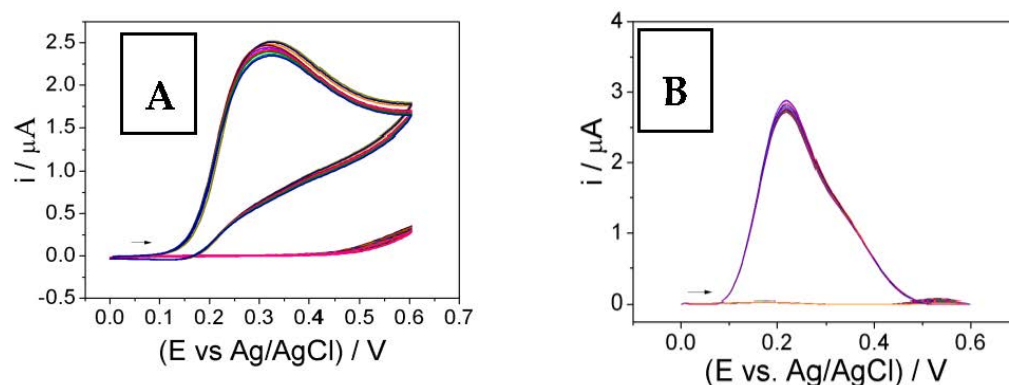


Figure 9. Cyclic voltammogram (A) and SWV (B) in the absence and presence of folate. The arrows indicate the direction of the scan

This result showed that the MMIPs/CPE-based analytical method proposed in this study exhibited excellent accuracy and steadiness when applied to the conduct of electrochemical measurements. In addition, it was also verified that the electrode surface can be polished five times and after this step, the amount of mass lost in the polishing must be replaced. From an analytical point of view, many analyses can be performed by replacing the modified paste with MMIP.

3.9. Interference Study

Figure 10 shows the results obtained from the interference analysis conducted using some potential interfering compounds in the presence of the analyte in different food samples. The analysis was performed using SWV with a concentration ratio of 1:1 which

was diluted 50 times for interferent and analyte, respectively. A larger sample addition was performed and it was verified that the ionic strength was altered by decreasing the electrochemical signal and, in this sense, the 50-fold dilution was used in the experiments. The objective of this study is to evaluate the potential interference of these compounds in the signal of the proposed sensor when applied for the detection of the analyte (folate).

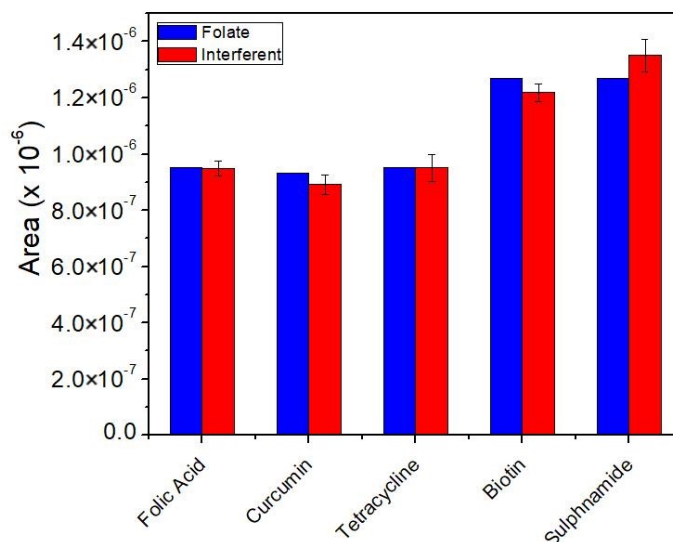


Figure 10. Interference analysis using the MMIP/CPE sensor in the presence of folate and other interfering compounds in the concentration range of 1:1.

The results obtained showed that the proposed sensor exhibited nearly 100% selectivity toward the detection of the analyte (folate) in the presence of other interfering compounds such as curcumin, tetracycline, biotin, and sulfonamide. The results obtained in this analysis point to the reliability of the proposed sensor when applied for the sensitive and selective determination of folate.

3.10. Application of the Proposed Sensor in Real Food Samples

One of the most important features of the MMIPs/CPE sensor is its fast response time, which makes it highly promising for application toward the detection of specific analytes. MMIPs are artificially synthesized materials employed for recognition components owing to their higher thermal stability, reusability, and selectivity compared to biological recognition receptors. Some important studies for the detection of an important analyte in real environmental samples using molecularly imprinted polymer (MIP) are present in the Supplementary Material, Table S1.

Under optimized conditions, the proposed sensor was applied for the detection of folate in real samples using the spiking method. The response obtained from the application of the proposed sensor for the detection of folate in different food products can be found in Table 2. See Figure S6 for additional results on the application of the proposed sensor before and after magnetic separation. The application of the proposed sensor yielded high recovery rates, with recovery percentages in the range of 92–108%. These results clearly show that the proposed analytical method is a highly efficient alternative that can be used for the successful determination of folate in different matrices. To further confirm the efficiency of the proposed technique, the sensor was also tested for the analysis of low folate concentration in oranges and broccoli. The results obtained pointed to the efficiency of the proposed sensor when applied for the detection of folate in different food samples. The application of the proposed sensor in this confirmation analysis yielded recovery rates in the range of 98–103% (Table 3).

Table 2. Results obtained from the application of the proposed sensor for the detection and recovery of folate in different food samples.

Food Samples	Added (mol L ⁻¹)	Found (mol L ⁻¹) *	Recovery (%) **	HPLC Method
beet	5.0×10^{-6}	$(4.8 \pm 0.2) \times 10^{-6}$	96	99.5
flour	5.0×10^{-6}	$(5.3 \pm 0.1) \times 10^{-6}$	107	102.2
cauliflower	5.0×10^{-6}	$(5.0 \pm 0.4) \times 10^{-6}$	100	101.6
orange	5.0×10^{-6}	$(4.6 \pm 0.1) \times 10^{-6}$	92	98.8
broccoli	5.0×10^{-6}	$(5.4 \pm 0.2) \times 10^{-6}$	108	97.67

* Average of 3 measured concentrations; ** Recovery percentage = $[\text{Found}]/[\text{Added}] \times 100$.

Table 3. Results obtained from the application of the proposed sensor for the detection of folate at low concentrations in other food samples (orange and broccoli).

Samples	Proposed Method		Recovery (%) **	HPLC Method
	Added ($\mu\text{mol L}^{-1}$)	Found * ($\mu\text{mol L}^{-1}$)		Recovery
Orange	2.0×10^{-7}	$(1.98 \pm 0.20) \times 10^{-7}$	99.0	98.92
	8.0×10^{-7}	$(7.85 \pm 0.30) \times 10^{-7}$	98.1	101.23
Broccoli	2.0×10^{-7}	$(2.04 \pm 0.25) \times 10^{-7}$	102.0	99.72
	8.0×10^{-7}	$(8.25 \pm 0.20) \times 10^{-7}$	103.1	100.92

* Average of 3 measured concentrations; ** Recovery percentage = $[\text{Found}]/[\text{Added}] \times 100$.

4. Conclusions

The present work reported the development and application of a novel, highly efficient MMIPs/CPE sensor for the sensitive and selective detection of folate in food products. The MMIPs/CPE sensor was developed using the core-shell method using magnetite nanoparticles, which were derived from the immersion of iron (III) acetylacetonate in tri-ethylene glycol (TEG) solvent via the application of the polyol method. The surface-imprinting strategy of the proposed electrode was devised using EDGMA as a cross-linking reagent and AIBN as a radical initiator.

The application of the composite MMIPs/CPE-based technique for the detection of folate showed that the proposed sensor has superior advantages over other techniques reported in the literature. The proposed sensor is found to be of low cost and has good stability. The sensor also exhibited a low detection limit with outstanding selectivity and good repeatability. Another remarkable advantage of the proposed sensing device is its ability to be reused for consecutive analyses by simply polishing the electrode surface. The MMIPs/CPE sensor has proven to be highly efficient when applied for the quantitation of folate in food samples.

Supplementary Materials: The following supporting information can be downloaded at: <https://www.mdpi.com/article/10.3390/chemosensors10110473/s1>, Figure S1: (a) Fundamental) three-dimensional structural formula; Figure S2: Experimental parameters applied in the formation of magnetite nanoparticles prepared by the polyol method; Figure S3: The plots about nitrogen adsorption; Figure S4: Analytical curve obtained from the application of the HPLC-UV method for the determination of different concentrations of folate. Analysis conditions: 0.1% phosphoric acid in a solution containing water and methanol; flow rate of 0.8 mL min⁻¹; column temperature of 25 °C; detection wavelength of 280 nm. Gradient elution: 0–7 min; Figure S5: Cyclic voltammograms obtained from the application of different electrodes. Measurements were performed using scan rate = 50 mVs⁻¹, acetate buffer solution (at pH 4.0) in the presence of 1.1×10^{-5} mol L⁻¹ folate; Figure S6: Analysis of real samples based on the application of the MIP/CPE sensor using different food samples. (a) Real food samples; (b) MMIPs before magnetic separation; (c) MMIPs after magnetic separation; Figure S7: Electrochemical determination of folate by SWV using the mag-MIP/CPE sensor. Analysis conditions: 0.1 mol L⁻¹ acetate buffer solution (pH 4.0). SWV conditions: $f = 15$ Hz, $a = 75$ mV, $\Delta E_s = 5$ mV, and folate concentration = 2.7×10^{-5} mol L⁻¹; Table S1: Optimized param-

ters of SWV for detection of folate; Table S2: Application of MMIPs for selective extraction of analytes from real samples. References [44–48] are cited in the Supplementary Materials.

Author Contributions: S.K., Methodology, Validation, Investigation, Writing—original draft, A.W., Investigation, Data curation, Methodology, Formal analysis, Writing—review & editing, technical support, M.R., Technical support, Corrections and suggestion, M.d.P.T.S., Supervision, Conceptualization, data curation, Project administration, Writing—review & editing, technical support, Writing—original draft. All authors have read and agreed to the published version of the manuscript

Funding: The authors are extremely grateful to the following research funding agencies for the financial assistance granted in support of this research: FAPESP (grants #2019/00677-7 and #2014/50945-4), CNPq (grants #151717/2018-4, #408050/2018 7, #301728/2019-4 and #465571/2014-0), and Capes (PROJ. AUX/PE/PROEX N° 0674/2018 CAPES)—Brazil and TUM Global Incentive Fund (Germany).

Institutional Review Board Statement: Not applicable.

Informed Consent Statement: Not applicable.

Data Availability Statement: The data presented in this study are available on request to the correspondence.

Acknowledgments: The authors are extremely grateful to the assistance from TUM Liaison Officer Sören Metz in São Paulo and to the Global Alliance of Bioeconomy UNESP (CAPES-PRINT).

Conflicts of Interest: The authors declare that they have no known competing financial interests or personal relationships that could have appeared to influence the work reported in this paper.

References

1. Hanson, A.D.; Gregory, J.F. Folate Biosynthesis, Turnover, and Transport in Plants. *Annu. Rev. Plant Biol.* **2011**, *62*, 105–125. [[CrossRef](#)]
2. Kopp, M.; Dürr, K.; Steigleder, M.; Clavel, T.; Rychlik, M. Measurements of Intra- and Extra-Cellular 5-Methyltetrahydrofolate Indicate that *Bifidobacterium Adolescentis* DSM 20083T and *Bifidobacterium Pseudocatenulatum* DSM 20438T Do Not Actively Excrete 5-Methyltetrahydrofolate In vitro. *Front. Microbiol.* **2017**, *8*, 445. [[CrossRef](#)] [[PubMed](#)]
3. Hjortmo, S.; Patring, J.; Jastrebova, J.; Andlid, T. Inherent biodiversity of folate content and composition in yeasts. *Trends Food Sci. Technol.* **2005**, *16*, 311–316. [[CrossRef](#)]
4. Jacob, F.F.; Striegel, L.; Rychlik, M.; Hutzler, M.; Methner, F.-J. Yeast extract production using spent yeast from beer manufacture: Influence of industrially applicable disruption methods on selected substance groups with biotechnological relevance. *Eur. Food Res. Technol.* **2019**, *245*, 1169–1182. [[CrossRef](#)]
5. Gorelova, V.; Bastien, O.; De Clerck, O.; Lespinats, S.; Rébeillé, F.; Van Der Straeten, D. Evolution of folate biosynthesis and metabolism across algae and land plant lineages. *Sci. Rep.* **2019**, *9*, 5731. [[CrossRef](#)] [[PubMed](#)]
6. van der Put, N.M.J.; Blom, H.J. Neural tube defects and a disturbed folate dependent homocysteine metabolism. *Eur. J. Obstet. Gynecol. Reprod. Biol.* **2000**, *92*, 57–61. [[CrossRef](#)]
7. Bailey, L.B.; Stover, P.J.; McNulty, H.; Fenech, M.F.; Gregory, J.F., III; Mills, J.L.; Pfeiffer, C.M.; Fazili, Z.; Zhang, M.; Ueland, P.M.; et al. Biomarkers of Nutrition for Development—Folate Review. *J. Nutr.* **2015**, *145*, 1636S–1680S. [[CrossRef](#)]
8. Snowdon, D.A.; Tully, C.L.; Smith, C.D.; Riley, K.P.; Markesbery, W.R. Serum folate and the severity of atrophy of the neocortex in Alzheimer disease: Findings from the Nun Study. *Am. J. Clin. Nutr.* **2000**, *71*, 993–998. [[CrossRef](#)]
9. Dugdale, A.E. Predicting iron and folate deficiency anaemias from standard blood testing: The mechanism and implications for clinical medicine and public health in developing countries. *Theor. Biol. Med. Model.* **2006**, *3*, 34. [[CrossRef](#)]
10. Saini, R.K.; Nile, S.H.; Keum, Y.-S. Folates: Chemistry, analysis, occurrence, biofortification and bioavailability. *Food Res. Int.* **2016**, *89*, 1–13. [[CrossRef](#)]
11. Menezo, Y.; Elder, K.; Clement, A.; Clement, P. Folic Acid, Folinic Acid, 5 Methyl TetraHydroFolate Supplementation for Mutations That Affect Epigenesis through the Folate and One-Carbon Cycles. *Biomolecules* **2022**, *12*, 197. [[CrossRef](#)] [[PubMed](#)]
12. Irvine, N.; England-Mason, G.; Field, C.J.; Dewey, D.; Aghajafari, F. Prenatal Folate and Choline Levels and Brain and Cognitive Development in Children: A Critical Narrative Review. *Nutrients* **2022**, *14*, 364. [[CrossRef](#)]
13. de Paiva, E.P.; Costa, M.M.A.; de Azevedo, C.A. Folate—Analytical properties, bioavailability and stability in foods. *Sci. Chromatogr.* **2015**, *7*, 199–222. [[CrossRef](#)]
14. McNulty, H.; Pentieva, K. Folate bioavailability. *Proc. Nutr. Soc.* **2004**, *63*, 529–536. [[CrossRef](#)]
15. Arcot, J.; Shrestha, A. Folate: Methods of analysis. *Trends Food Sci. Technol.* **2005**, *16*, 253–266. [[CrossRef](#)]
16. Ringling, C.; Rychlik, M. Origins of the difference between food folate analysis results obtained by LC–MS/MS and microbiological assays. *Anal. Bioanal. Chem.* **2017**, *409*, 1815–1825. [[CrossRef](#)] [[PubMed](#)]
17. Vishnumohan, S.; Arcot, J.; Pickford, R. Naturally-occurring folates in foods: Method development and analysis using liquid chromatography–tandem mass spectrometry (LC–MS/MS). *Food Chem.* **2011**, *125*, 736–742. [[CrossRef](#)]

18. Ložnjak, P.; Striegel, L.; Díaz De la Garza, R.I.; Rychlik, M.; Jakobsen, J. Quantification of folate in food using deconjugase of plant origin combined with LC-MS/MS: A method comparison of a large and diverse sample set. *Food Chem.* **2020**, *305*, 125450. [[CrossRef](#)]
19. Yin, S.; Yang, Y.; Li, Y.; Sun, C. Analysis of natural and synthetic folates in pharmaceuticals and foods: A review. *Anal. Methods* **2018**, *10*, 9–21. [[CrossRef](#)]
20. Uzuriaga-Sánchez, R.J.; Khan, S.; Wong, A.; Picasso, G.; Pividori, M.I.; Sotomayor, M.D.P.T. Magnetically separable polymer (Mag-MIP) for selective analysis of biotin in food samples. *Food Chem.* **2016**, *190*, 460–467. [[CrossRef](#)]
21. Tang, H.; Zhu, L.; Yu, C.; Shen, X. Selective photocatalysis mediated by magnetic molecularly imprinted polymers. *Sep. Purif. Technol.* **2012**, *95*, 165–171. [[CrossRef](#)]
22. Chen, L.; Zhang, X.; Xu, Y.; Du, X.; Sun, X.; Sun, L.; Wang, H.; Zhao, Q.; Yu, A.; Zhang, H.; et al. Determination of fluoroquinolone antibiotics in environmental water samples based on magnetic molecularly imprinted polymer extraction followed by liquid chromatography-tandem mass spectrometry. *Anal. Chim. Acta* **2010**, *662*, 31–38. [[CrossRef](#)] [[PubMed](#)]
23. Chen, L.; Zhang, X.; Sun, L.; Xu, Y.; Zeng, Q.; Wang, H.; Xu, H.; Yu, A.; Zhang, H.; Ding, L. Fast and selective extraction of sulfonamides from honey based on magnetic molecularly imprinted polymer. *J. Agric. Food Chem.* **2009**, *57*, 10073–10080. [[CrossRef](#)]
24. Santos, A.C.F.; de Araújo, O.R.; Moura, F.A.; Khan, S.; Tanaka, A.A.; Santana, A.E.G.; Pividori, M.I.; Taboada-Sotomayor, M.D.P.; Goulart, M.O. Development of magnetic nanoparticles modified with new molecularly imprinted polymer (MIPs) for selective analysis of glutathione. *Sens. Actuators B Chem.* **2021**, *344*, 130171. [[CrossRef](#)]
25. Garcia, S.M.; Wong, A.; Khan, S.; Sotomayor, M.D. A simple, sensitive and efficient electrochemical platform based on carbon paste electrode modified with Fe₃O₄@MIP and graphene oxide for folic acid determination in different matrices. *Talanta* **2021**, *229*, 122258. [[CrossRef](#)] [[PubMed](#)]
26. Pizan-Aquino, C.; Wong, A.; Avilés-Félix, L.; Khan, S.; Picasso, G.; Sotomayor, M.D.P.T. Evaluation of the performance of selective M-MIP to tetracycline using electrochemical and HPLC-UV method. *Mater. Chem. Phys.* **2020**, *245*, 122777. [[CrossRef](#)]
27. Chen, L.; Liu, J.; Zeng, Q.; Wang, H.; Yu, A.; Zhang, H.; Ding, L. Preparation of magnetic molecularly imprinted polymer for the separation of tetracycline antibiotics from egg and tissue samples. *J. Chromatogr. A* **2009**, *1216*, 3710–3719. [[CrossRef](#)]
28. Sotomayor, M.D.P.T.; Kubota, L.T. Enzymeless biosensors: Uma nova área para o desenvolvimento de sensores amperométricos. Enzymeless biosensors: A novel area for the development of amperometric sensors. *Quím. Nova* **2002**, *25*, 123–128. [[CrossRef](#)]
29. Wong, A.; Santos, A.M.; Silva, T.A.; Moraes, F.C.; Fatibello-Filho, O.; Sotomayor, M.D.P.T. Sensitive and Selective Voltammetric Determination of Ciprofloxacin Using Screen-printed Electrodes Modified with Carbon Black and Magnetic-molecularly Imprinted Polymer. *Electroanalysis* **2022**, *34*, 1–11. [[CrossRef](#)]
30. Dou, W.-T.; Han, H.-H.; Sedgwick, A.C.; Zhu, G.-B.; Zang, Y.; Yang, X.-R.; Yoon, J.; James, T.D.; Li, J.; He, X.-P. Fluorescent probes for the detection of disease-associated biomarkers. *Sci. Bull.* **2022**, *67*, 853–878. [[CrossRef](#)]
31. Ding, S.; Lyu, Z.; Li, S.; Ruan, X.; Fei, M.; Zhou, Y.; Niu, X.; Zhu, W.; Du, D.; Lin, Y. Molecularly imprinted polypyrrole nanotubes based electrochemical sensor for glyphosate detection. *Biosens. Bioelectron.* **2021**, *191*, 113434. [[CrossRef](#)] [[PubMed](#)]
32. Vega-Chacón, J.; Picasso, G.; Avilés-Félix, L.; Jafellici, M. Influence of synthesis experimental parameters on the formation of magnetite nanoparticles prepared by polyol method. *Adv. Nat. Sci. Nanosci. Nanotechnol.* **2016**, *7*, 015014. [[CrossRef](#)]
33. Villa, J.E.L.; Khan, S.; Neres, L.C.S.; Sotomayor, M.D.P.T. Preparation of a magnetic molecularly imprinted polymer for non-invasive determination of cortisol. *J. Polym. Res.* **2021**, *28*, 298. [[CrossRef](#)]
34. Khan, S.; Wong, A.; Zaroni, M.V.B.; Sotomayor, M.D.P.T. Sotomayor. Electrochemical sensors based on biomimetic magnetic molecularly imprinted polymer for selective quantification of methyl green in environmental samples. *Mater. Sci. Eng. C* **2019**, *103*, 109825. [[CrossRef](#)] [[PubMed](#)]
35. Miguel-Sancho, N.; Bomati-Miguel, O.; Roca, A.G.; Martinez, G.; Arruebo, M.; Santamaria, J. Molecularly Imprinted Polymers for Gossypol via Sol-Gel, Bulk, and Surface Layer Imprinting—A Comparative Study. *Polymers* **2019**, *11*, 602.
36. Miguel-Sancho, N.; Bomati-Miguel, O.; Roca, A.G.; Martinez, G.; Arruebo, M.; Santamaria, J. Synthesis of Magnetic Nanocrystals by Thermal Decomposition in Glycol Media: Effect of Process Variables and Mechanistic Study. *Ind. Eng. Chem. Res.* **2012**, *51*, 8348–8357. [[CrossRef](#)]
37. Yang, T.; Shen, C.; Li, Z.; Zhang, H.; Xiao, C.; Chen, S.; Xu, Z.; Shi, D.; Li, J.; Gao, H. Highly Ordered Self-Assembly with Large Area of Fe₃O₄ Nanoparticles and the Magnetic Properties. *J. Phys. Chem. B* **2005**, *109*, 23233–23236. [[CrossRef](#)]
38. Quinto, M.L.; Khan, S.; Picasso, G.; Sotomayor, M.D.P.T. Synthesis, characterization, and evaluation of a selective molecularly imprinted polymer for quantification of the textile dye acid violet 19 in real water samples. *J. Hazard. Mater.* **2019**, *384*, 121374. [[CrossRef](#)]
39. Li, Y.; Li, X.; Chu, J.; Dong, C.; Qi, J.; Yuan, Y. Synthesis of core-shell magnetic molecular imprinted polymer by the surface RAFT polymerization for the fast and selective removal of endocrine disrupting chemicals from aqueous solutions. *Environ. Pollut.* **2010**, *158*, 2317–2323. [[CrossRef](#)]
40. Kong, X.; Gao, R.; He, X.; Chen, L.; Zhang, Y. Synthesis and characterization of the core-shell magnetic molecularly imprinted polymers (Fe₃O₄@MIPs) adsorbents for effective extraction and determination of sulfonamides in the poultry feed. *J. Chromatogr. A* **2012**, *1245*, 8–16. [[CrossRef](#)]
41. Zaitsev, V.S.; Filimonov, D.S.; Presnyakov, I.A.; Gambino, R.J.; Chu, B. Physical and Chemical Properties of Magnetite and Magnetite-Polymer Nanoparticles and Their Colloidal Dispersions. *J. Colloid Interface Sci.* **1999**, *212*, 49–57. [[CrossRef](#)] [[PubMed](#)]

42. Popplewell, J.; Sakhnini, L. The dependence of the physical and magnetic properties of magnetic fluids on particle size. *J. Magn. Magn. Mater.* **1995**, *149*, 72–78. [[CrossRef](#)]
43. Kodama, R.H.; Berkowitz, A.E.; McNiff, E.J., Jr.; Foner, S. Surface Spin Disorder in NiFe₂O₄ Nanoparticles. *Phys. Rev. Lett.* **1996**, *77*, 394–397. [[CrossRef](#)] [[PubMed](#)]
44. Chekin, F.; Teodorescu, F.; Coffinier, Y.; Pan, G.H.; Barras, A.; Boukherroub, R.; Szunerits, S. MoS₂/Reduced Graphene Oxide as Active Hybrid Material for the Electrochemical Detection of Folic Acid in Human Serum. *Biosens. Bioelectron.* **2016**, *85*, 807–813. [[CrossRef](#)] [[PubMed](#)]
45. Arvand, M.; Dehsaraei, M. A Simple and Efficient Electrochemical Sensor for Folic Acid Determination in Human Blood Plasma Based on Gold Nanoparticles-Modified Carbon Paste Electrode. *Mater. Sci. Eng. C* **2013**, *33*, 3474–3480. [[CrossRef](#)]
46. Taherkhani, A.; Jamali, T.; Hadadzadeh, H.; Karimi-Maleh, H.; Beitollahi, H.; Taghavi, M.; Karimi, F. ZnO Nanoparticle-Modified Ionic Liquid-Carbon Paste Electrode for Voltammetric Determination of Folic Acid in Food and Pharmaceutical Samples. *Ionics* **2014**, *20*, 421–429. [[CrossRef](#)]
47. Khaleghi, F.; Irai, A.E.; Sadeghi, R.; Gupta, V.K.; Wen, Y.P. A Fast Strategy for Determination of Vitamin B9 in Food and Pharmaceutical Samples Using an Ionic Liquid-Modified Nanostructure Voltammetric Sensor. *Sensors* **2016**, *16*, 747. [[CrossRef](#)]
48. D'Souza, O.J.; Mascarenhas, R.J.; Satpati, A.K.; Detriche, S.; Mekhalif, Z.; Delhalle, J. High Electrocatalytic Oxidation of Folic Acid at Carbon Paste Electrode Bulk Modified with Iron Nanoparticle-Decorated Multiwalled Carbon Nanotubes and Its Application in Food and Pharmaceutical Analysis. *Ionics* **2017**, *23*, 201–212. [[CrossRef](#)]